Optical and mechanical shrinkage effects in dye-doped photonic bandgap structures based on organic materials

D. Lucchetta,[1] O. Francescangeli,[1] L. Criante,[1] F. Simoni,[1] L. Pierantoni,[2] T. Rozzi,[2] M. Scoponi,[3] and S. Rossetti[3]
[1]*Dipartimento di Fisica e Ingegneria dei Materiali e del Territorio and CNISM, Università Politecnica delle Marche, via Brecce Bianche, 60131 Ancona, Italy*
[2]*Dipartimento di Elettromagnetismo e Bioingegneria, Università Politecnica delle Marche, via Brecce Bianche, 60131 Ancona, Italy*
[3]*Istituto per la Sintesi Organica e la Fotoreattività del C.N.R. (ISOF-CNR), sez. Ferrara, Dipartimento di Chimica dell'Università, Via Borsari, 46-44100 Ferrara, Italy*
(Received 8 September 2005; published 23 January 2006)

In this work we study the effects of the optical shrinkage in polymer and liquid crystal (LC) mixtures optimized for their use as active media in compact plastic laser devices. These mixtures are characterized by the presence of the rhodamine 6G as an active dye. Modifications in the reflection properties of the gratings as a function of the active dye concentration have been determined experimentally and a detailed theoretical simulation of the optical transmittance properties of these devices is provided. Moreover, the comparison between two different experimental approaches clarifies the contribution to the optical shrinkage due to the presence of the active dye. In principle this approach allows determining the linear mechanical shrinkage by separating the contribution to optical shrinkage due to photochemical transformations from that due to mechanical effects.

DOI: 10.1103/PhysRevE.73.011708 PACS number(s): 61.30.−v, 78.40.Me, 42.40.−i, 02.70.−c

I. INTRODUCTION

Interest in the fabrication of small organic optical devices operating in the visible range of the electromagnetic spectrum is constantly growing. Different applications can be found starting from one dimensional (1D) filters, switchable elements for diffractive optics [1], reflective color displays [2] up to compact one dimensional [3–5] or two dimensional [6] optical resonators, and plastic laser sources. Several other devices are currently in advanced phase of realization, e.g., electrically switchable multidimensional filters, laser devices for wavelength multiplexing and de-multiplexing, active devices for multiwavelengths output and multidirectional spatial addressing, high resolution reflection gratings for holographic data storage, and compact tunable laser source for optical pickups. Many of these devices are based on periodic structures recorded by means of conventional optical holographic techniques in organic materials named holographic polymer dispersed liquid crystals (HPDLCs) [1]. HPDLCs are a well known class of photosensitive composite materials constituted by a photopolymerizable mixture of monomers and liquid crystal (LC) molecules. Transmission and/or reflection gratings can be easily written in HPDLC material by a simple "one-step" process. We refer to these configurations as photonic bandgap (PBG) structures with one (1D) or more (2D, 3D) spatial dimensions. Along any spatial direction the grating pitch can be selected from a wide range of values by varying the angle of incidence of the writing beams and/or the writing wavelength. Unfortunately, the conversion of monomer molecules into a polymer network is generally characterized by a strong packing of the growing polymer chains with consequent volume contraction called "polymerization shrinkage." It has been recently demonstrated that shrinkage phenomena depend on the effective functionality of the oligomers and/or monomers of the light curable mixtures [7]. Optical shrinkage plays an important role in determining the operating wavelength of the devices based on holographic gratings. With the aim of achieving better understanding of this role in this work we study the effects of the optical shrinkage in polymer-LC mixtures optimized for their use as active media in compact plastic laser devices based on high-resolution reflection gratings [4]. These mixtures are characterized by the presence of rhodamine 6G as an active dye. Modifications in the reflection properties of the gratings as a function of the active dye concentration have been experimentally determined and a detailed theoretical simulation of the transmission and reflection properties, which includes absorption, is provided. Moreover, the comparison between two different experimental approaches clarifies the contribution to the optical shrinkage due to the presence of the active dye. In principle this approach allows the determination of the linear mechanical shrinkage by separating the contribution to optical shrinkage due to photochemical transformations from that due to mechanical effects.

II. EXPERIMENTAL PROCEDURES AND SAMPLE PREPARATION TECHNIQUES

A key feature of an organic distributed feedback (DFB) device is the reflection grating based on HPDLC. It was realized by exposing for 5 min an isotropic monomer-liquid crystal photosensitive mixture to the interference pattern of two *s*-polarized Ar^{++} ion laser beams with $\lambda=476.5$ nm and intensity $I=150\ \mathrm{mW/cm^2}$ per beam. The resulting spatial pitch is about $\Lambda=0.2\ \mu$m. The short period is an essential requirement for the reflection grating to work in the visible spectrum. The grating wave vector $\mathbf{K}$ ($K=2\pi/\Lambda$) is normal to the glass surfaces. The pre-polymer mixture was a solution of (i) the monomer dipentaerythritol hydroxy pentaacrylate DPHPA, (ii) LC BL038 from Merck, and (iii) a mixture of

 ©2006 The American Physical Society

the photoinitiator Rose Bengale RB and the coinitiator N-phenyglycine (NPG) dissolved in the cross-linking monomer N-vinylpyrrollidone (NVP) (4% RB, 10% NPG). The chemical structure of the components was reported elsewhere [8]. The weight ratio of the DPHPA, LC, and photoinitiator mixture was 50:36:14. The mixture was sandwiched between two 1-mm-thick glass substrates and the cell thickness d was controlled by using two 13-μm mylar stripes. $1-6\times10^{-2}$-M solutions of the active dye rodamine 6G were realized by using our starting isotropic mixture as solvent. A writing wavelength of $\lambda=476.5$ was selected for our reflection grating to avoid photobleaching of the rhodamine 6G dye during the irradiation process [4]. The optical characterization of the grating was performed by measuring its transmission spectrum. The measurements were carried out by illuminating the HPDLC gratings through an optical fiber with an incoherent tungsten light source emitting in the wavelength range 350–1000 nm, and collecting the transmitted light through an optical fiber connected to a monochromator. The photopolymerization kinetics of the visible-light curable (VLC) mixtures was carried out by using a modified DTA Mettler 820 differential scanning calorimeter calibrated with indium and equipped with liquid nitrogen reservoir and a Hamamatsu xenon lamp (model LC5) with a quartz bifurcated fiber bundle in order to transfer the light beam into the reference and sample pans. The photo-DSC measurements were carried out on an 8–10-mg sample of the VLC mixtures inserted in an aluminium pan by measuring the heat flow as a function of the visible light irradiation time. A shutter in front of the glass fiber entrance, driven by the interfaced personal computer, was used to regulate the irradiation time under isothermal conditions (25 °C). The samples were kept 1 min in the dark for conditioning and then irradiated for 150 s under isothermal conditions. The intensity of the filtered incident light at 456 nm, measured by using a Macam radiometer, was maintained constant at 33 mW/cm^2 for every photopolymerization experiment.

The linear mechanical shrinkage was evaluated by using a fast oscillating rotational rheometer of Reologica (model Stresstech) equipped with a Hamamatsu xenon lamp and a quartz grade fiber bundle. The visible light irradiation of the samples was achieved by replacing the lower plate in the rheometer with a quartz window close to the optical fiber exit. A computer controlled shutter sets the xenon lamp irradiation time. The shear mechanical modulus (G') and the dissipative shear mechanical modulus (G'') of the VLC samples were monitored as a function of the irradiation time. All experiments were performed at 25 °C on a plate-to-plate fixture with a diameter of 8 mm, the initial gap between the two plates was of 50 μm and the intensity of the filtered visible light at 456 nm was 33 mW/cm^2. A pre-shearing stress of 4 Pa was applied to the VLC samples to avoid artifacts due to the delamination from the plates or to the formation of voids.

III. THEORY

A. Transmission matrix method

The analyzed physical structure consists of the periodic alternation of polymer and liquid crystal layers, sandwiched between two glass plates as shown in Fig. 1. By referring to the rectangular coordinate systems of Fig. 1, the structure is periodically stratified along the z direction, with grating pitch Λ and overall length d. The other two sides (of length l) lie on the transverse plane. The thickness of the two glass layers is t_g and the refractive index n_g. The polymer and LC layers have thickness h_P and h_{CL}, respectively; setting $h_P=L$ we have $h_{CL}=\Lambda-L$. The refractive indices are n_P and n_{CL}, respectively. The exciting laser beam is represented by an electromagnetic (EM) plane wave with frequency $\omega=\omega_0$ propagating along z, with the electric field linearly polarized in the transverse (xy) plane:

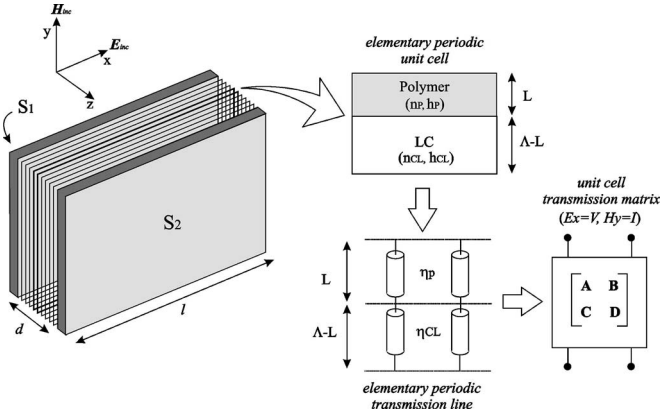

FIG. 1. The analyzed periodic structure which consists of the alternation of polymer and LC layers, sandwiched between two glass plates (S_1 and S_2), the elementary periodic transmission line characterized by the two characteristic impedances η_P and η_{CL}, and the equivalent unit cell transmission matrix with $E_x=V$ and $H_y=I$.

$$\vec{E}_{inc}=\vec{E}_0e^{j\omega t}=E_0e^{j\omega_0 t}\hat{x},\quad \vec{H}_{inc}=\frac{1}{\eta_0}(\hat{z}\times\vec{E})=H_0e^{j\omega_0 t}\hat{y}, \tag{1}$$

where $\eta=(\mu_0/\varepsilon_0)^{1/2}$ is the free-space impedance. In order to simplify the mathematical treatment, we used the same notation indicated in Ref. [9]. Since the condition $l\gg d$ is fulfilled and the spot size of the beam is considered small compared to l, we reduce the EM analysis to a 1D plane-wave propagation problem in a terminated periodic structure. By making the approximation of $l\to\infty$, we use the computational transmission matrix ($ABCD$) technique [9,10]. This method is based on modeling 1D propagation by an equivalent cascade of transmission lines which naturally leads to the methods of classical circuit theory of microwave and optical networks. In the present case, the amplitude of the transverse electric field is proportional to the voltage in the equivalent network and the amplitude of the transverse magnetic field is proportional to the current. The overall transmission matrix is easily obtained by the cascade multiplication of individual (2×2) transmission matrices as reported in the following paragraph.

B. Analysis of the periodic structure

The elementary unit cell of the periodic structure is constituted by one layer of polymer followed by one of liquid

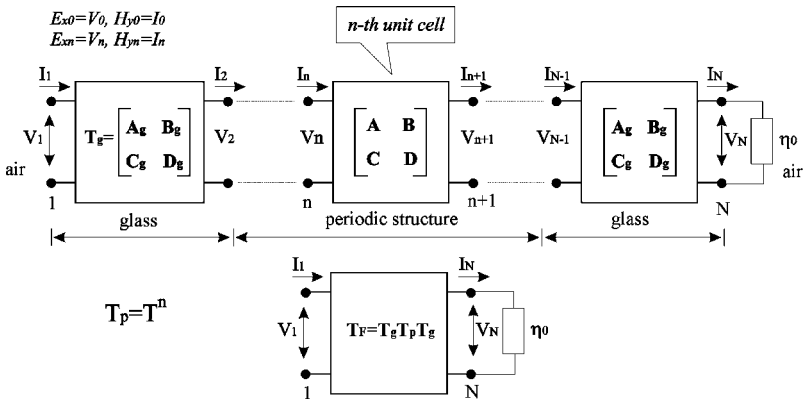

FIG. 2. Equivalent network representation of the periodic structure of Fig. 1.

crystal. The total thickness d, from the end of the first glass layer to the beginning of the second one (see Figs. 1 and 2) involves the cascade of N unit cells with a grating pitch Λ. Alternating dielectric layers with different refractive indices are modeled as alternating sections of transmission line of different characteristic impedances:

$$\eta_1 = \eta_P = \sqrt{\mu_0/\varepsilon_1}, \quad \eta_2 = \eta_{CL} = \sqrt{\mu_0/\varepsilon_2}, \tag{2}$$

where ε_1 and ε_2 are the polymer and LC refractive indices, respectively. The corresponding transmission matrix, of the nth unit cell (see Fig. 2) relates voltages V (electric-field component) and currents I (magnetic-field component), defined at the end planes of each unit cell:

$$\begin{bmatrix} V_n \\ I_n \end{bmatrix} = \begin{bmatrix} A & B \\ C & D \end{bmatrix} \begin{bmatrix} V_{n+1} \\ I_{n+1} \end{bmatrix} = [\mathbf{T}] \begin{bmatrix} V_{n+1} \\ I_{n+1} \end{bmatrix} \Leftrightarrow \begin{bmatrix} V_{n+1} \\ I_{n+1} \end{bmatrix}$$
$$= [\mathbf{T}]^{-1} \begin{bmatrix} V_n \\ I_n \end{bmatrix}, \quad V_n = E_{x_n}, \quad I_n = H_{x_n}$$

$$A = \cos\theta_1 \cos\theta_2 - \frac{\eta_1}{\eta_2} \sin\theta_1 \sin\theta_2,$$
$$B = j\eta_2 \cos\theta_1 \sin\theta_2 + j\eta_1 \sin\theta_1 \sin\theta_2,$$
$$C = \frac{j}{\eta_2} \sin\theta_1 \cos\theta_2 + \frac{j}{\eta_2} \cos\theta_1 \sin\theta_2,$$
$$D = -\frac{\eta_2}{\eta_1} \sin\theta_1 \sin\theta_2 + \cos\theta_1 \cos\theta_2, \tag{3}$$

where $\eta_{1,2}$ are characteristic impedances of the transmission line, $k_{1,2}$ the wave numbers of the equivalent lines, and $\theta_{1/2}$ the electrical lengths. The corresponding eigenvalue equation for the complex propagation constant γ is then

$$\cosh(\gamma\Lambda) = \frac{A+D}{2}. \tag{4}$$

Once the spectral matrix is obtained, we can perform a canonical decomposition in diagonal form [10] and easily compute the total transmission matrix $\mathbf{T}_p$ of the cascaded n-unit cells as $\mathbf{T}_p = \mathbf{T}^n$. The latter is then pre- and post-multiplied by the $ABCD$ matrix of the glass layers $\mathbf{T}_g$,

$$[\mathbf{T}_g] = \begin{bmatrix} \cos\theta_g & j\eta_g \sin\theta_g \\ \frac{j}{\eta_g} \sin\theta_g & \cos\theta_g \end{bmatrix}, \tag{5}$$

where θ_g, η_g, k_g are the equivalent transmission line parameter for the glass thus forming the final matrix $\mathbf{T}_F = \mathbf{T}_g\mathbf{T}_p\mathbf{T}_g$. Port-1 of the resulting chain $\mathbf{T}_F$ is fed by the source voltage V_1, representing the impinging plane wave. The end port is loaded by the free-space impedance η_0, the air termination, as shown in Fig. 2. In order to compute the transmission coefficient S_{21} of the final equivalent circuit, it is convenient to normalize its $ABCD$ elements by η_0. Finally, the desired power transmission coefficient is obtained as

$$T_{power}(\omega) = \frac{P_{out}(\omega)}{P_{in}(\omega)} = |S_{21}(\omega)|^2, \quad S_{21} = \frac{2}{A+B+C+D}, \tag{6}$$

where $P_{out/in}$ is the modulus of the Poynting vector.

C. Debye model for absorption losses

We consider linear isotropic materials including the effect of losses on the response to the applied fields. Losses can affect the response to either electric or magnetic field, or both. As in the present materials, the magnetic response is very weak and the permeability is real and constant, we concentrate our investigation on the electric permittivity. The contribution to the total current density from bound electrons is $\mathbf{J} = j\omega(\varepsilon' - j\varepsilon'')\mathbf{E}$ whereas the conduction contribution $\mathbf{J} = \sigma\mathbf{E}$ is assumed to be negligible. The complex permittivity enters Maxwell's equations, thus modifying the propagation constants θ_i and impedances η_i of the elementary equivalent lines in Eqs. (2) and (5). Both ε' and ε'' are frequency dependent and physically related to the polarization vector $\mathbf{P}$, that enters the relation between $\mathbf{D}$ (electric flux density) and $\mathbf{E}$:

$$\vec{\nabla} \times \vec{H} = j\omega\vec{D}, \quad \vec{D} = \varepsilon_0\vec{E} + \vec{P} = \varepsilon_0(1+\chi_e)\vec{E}, \quad \chi_e = \frac{N\alpha_T g}{\varepsilon_0}. \tag{7}$$

The term χ_e is the dielectric susceptibility and we have assumed that the polarization is linearly dependent on the field $\mathbf{E}$. N is the number of molecules per unit volume, α_T is the

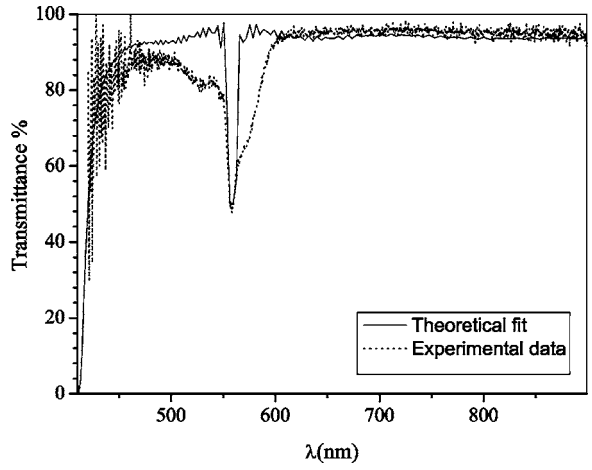

FIG. 3. Typical transmission spectrum of a HPDLC reflection grating. The dashed line represents the experimental data. The continuous line represents the theoretical simulation obtained with the transmission matrix method (l=0.5 mm, tg=1 mm).

molecular polarizability, and g is the ratio [12] between local field $\mathbf{E}_{\mathrm{loc}}$ acting on the molecule and the applied field $\mathbf{E}$. If the surrounding molecules act in a spherically symmetric fashion on the molecule for which $\mathbf{E}_{\mathrm{loc}}$ is being calculated, $g=(\chi_e+3)/3$ and we can write, according to the Clausius-Mossotti relation and to the Debye model [11,12]:

$$\frac{\chi_e}{\chi_e+3}=\frac{N\alpha_T(\omega)}{3\varepsilon_0},\quad \alpha_T(\omega)=\alpha_e(\omega)+\alpha_i(\omega)+\alpha_d(\omega),$$

$$\alpha_T(\omega)=\alpha_T'(\omega)-j\alpha_T''(\omega)\Rightarrow n_c(\omega)=\{[\varepsilon'(\omega)-j\varepsilon''(\omega)]/\varepsilon_0\}^{1/2}. \tag{8}$$

As shown in Eq. (8), several atomic and molecular effects contribute to the molecular polarizability α_T, and the refractive index n_c features frequency-dependent contributions from several different atomic or molecular effects. The electronic contribution α_e arises from the shift of the electron cloud in each atom relative to its positive nucleus. The ionic contribution α_i comes from the displacement of positive and negative ions from their neutral positions. Another contribution, α_d may arise if the individual molecules have permanent dipole moments as application of the electric field tends to align these permanent dipoles against the randomizing forces of molecular collision. Since random motion is a function of temperature, this last effect is clearly temperature dependent. In the classical Lorentian model each contribution to both electronic and ionic polarizabilities can be written as [11,12]

$$\alpha_n(\omega)=\alpha'_n(\omega)-j\alpha''_n(\omega)=\frac{A_n}{(\omega_n^2-\omega^2)+j\omega\Gamma_n},\quad n=T,e,i,d, \tag{9}$$

where ω_0 is the resonant frequency, A_n measures the strength of the nth resonance and Γ_n is damping coefficient. This has the form of the impedance of a parallel resonant circuit. Real and imaginary parts of the expression contribute to ε' and ε'', respectively. Near a resonance, losses represented by ε'' go through a peak while ε', like the reactance of the tuned circuit, displays peaks of opposite sign at either side of the resonance. The analytic properties of the complex permittivity provide relationships between ε' and ε'', known as Kramers-Kronig relations [12]. At optical frequencies both the ionic α_i and the permanent dipole moments α_d are negligible; also the electronic contributions are small, except in or near absorption bands, where they are a strong function of the wavelength [12]. This is just what happens in the HPDLC structure under analysis, where resonances due to absorption losses strongly affect the transmittivity, in particular in the presence of rhodamine. In fact HPDLC without rhodamine exhibits an absorption peak around 407 nm; in HPDLC with rhodamine we have three absorption peaks (peaks of resonance of ε'') 380, 510, and 530 nm. In particular the strong losses in the range 500–540 nm affect the passband-stopband characteristics, which is also interesting for possible applications to optical filtering.

D. Photocalorimetry (photo-DSC)

The expected polymerization heat (ΔH_0), i.e., the photopolymerization enthalpy in J/g, for the VLC samples was calculated by the following equation [13,14]:

$$\Delta H_0=\sum_i \frac{n_i w_i \Delta H_0^i}{M_i}\ \text{ in J/g with } i=1,2,\ldots,n, \tag{10}$$

where n_i takes into account the acrylic group numbers in the monomer or in oligomer chain ends, w_i is the sample weight fraction, ΔH_0^i is the theoretical polymerization heat for an acrylate monomer, and M_i is the molecular weight for the ith component in the curable mixture. The enthalpy of a photoinitiated polymerization at complete conversion for the acrylate monomers has been assumed to be 80.0 kJ/mol as reported elsewhere [15]. The expected (theoretical) polymerization heat, i.e., at complete conversion (p_t=1) by using Eq. (10) for the studied mixtures was calculated to be 370 J g^{-1}. The conversion degree (p_t) at 25 °C for the VLC mixtures as a function of the irradiation time t was calculated by dividing the experimentally measured polymerization heat (ΔH^t) in J/g, by the theoretical polymerization heat, ΔH_0:

$$p_t=\frac{\Delta H^t}{\Delta H^0}. \tag{11}$$

The photopolymerization rates, $R_p=-d[M]_t/dt$, of the VLC samples as a function of the irradiation time were calculated by using the following equation [13–16]:

$$\frac{R_p}{[M]_0}=\frac{dp_t}{dt}\ \text{ in } s^{-1}, \tag{12}$$

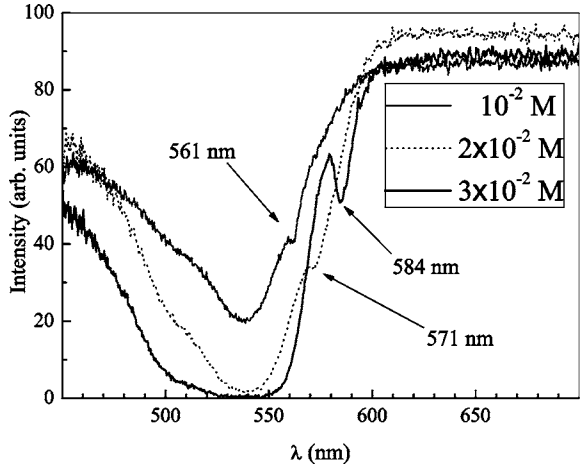

FIG. 4. Transmission spectra of HPDLC reflection gratings as function of the rhodamine 6G concentration from 1 to 3×10^{-2} M.

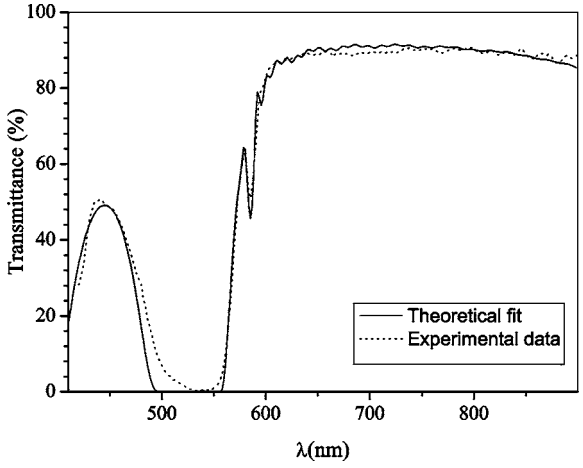

FIG. 5. Typical transmission spectrum of a HPDLC reflection grating containing a 3×10^{-2}-M solution of the rhodamine 6G dye. The dashed line represents the experimental data. The continuous line represents the theoretical simulation obtained with the transmission matrix method.

where $[M]_0$ was the initial reactive group concentration ($t=0$) expressed in mmol g^{-1}, while $[M]_t=[M]_0(1-p_t)$ was the residual monomer concentration at time t and dp_t/dt values were calculated by the numerical derivative of the conversion degree values obtained by Eq. (12). A relative standard error of 8% for the kinetic measurements was calculated by five independent measurements for every VLC sample under the same experimental conditions. The composition of the initial polymerizable group concentration ($[M]_0$) was 4.6 mmol g^{-1} in both visible light curable samples.

E. Photorheology

The VLC samples were loaded on the quartz lower plate and a preshear with an initial gap of 50 μm was applied to the samples. The dynamic shear moduli (G' and G'') measured at a frequency of 2 Hz and a fast oscillating shear stress were programmed to increase from 0.5 to 10 kPa by using a sigmoidal equation as a function of the visible light irradiation time. Initially a rapid increase of the shear moduli (G' and G'') with the sample irradiation was observed and the software was programmed to control the gap settings when the gel point was reached (i.e., $G'=G''$ or $\tan\delta=G''/G'=1$) [17]. Under these conditions the complex viscoelastic response of the samples exerting axial normal forces to the upper plate (i.e., autotension mode) were used to monitor the gap changes as a function of the visible light exposure. The shrinkage of the sample was measured quantitatively using the gap measurements as a function of the irradiation time. The total applied strain of 9% was within the linear viscoelastic range for both samples. A relative standard error of 11% for the rheological measurements was calculated by five independent measurements for every VLC sample under the same experimental conditions.

IV. EXPERIMENTAL RESULTS AND DISCUSSIONS

The typical transmission spectrum of a high resolution reflection hologram is shown by the dashed line of Fig. 3. The reflection peak due to the photo-induced periodic structure is clearly visible. In absence of shrinkage its position can be easily determined from the knowledge of the average refractive index of the mixture deriving from the material parameters. In our case, starting from the known values of the ordinary and extraordinary refractive indices of the LC, n_o and n_e, respectively, it is possible to calculate the average refractive index of the LC as

$$n_{LC}=\sqrt{\frac{2n_o^2+n_e^2}{3}}. \tag{13}$$

From the knowledge of the polymer refractive index after the photopolymerization process it is also possible to calculate the grating refractive index by using the following equation [18]:

$$n_G=\sqrt{n_{LC}^2\phi_{LC}+n_p^2\phi_p}, \tag{14}$$

where ϕ_{LC} and ϕ_p are the volume fractions of LC and polymer and n_p the refractive index of the polymer. Finally the position of the reflection peak can be evaluated by using the Bragg law for normal incidence: $\lambda_r=2n_G\Lambda$. In our case, with an external incidence angle (half angle between the two writing beams) $\theta=23.5°$ and a grating index $n_G=1.554$ (calculated taking into account the beam deflections due to the glass substrates and to the presence of the polymerizing material and a supposed 1% change in the refractive index [7] due to the photopolymerization process), the expected reflection wavelength is $\lambda_r\sim600$ nm. Due to the high shrinkage effects the real position of this peak is located at $\lambda_r=558$ nm. In the absence of active dye in the starting mixture, a 7% optical shrinkage has then been evaluated. In the same figure the continuous line represents the theoretical simulation of the reflection properties of the HPDLC grating made with the following parameters: $\Lambda=0.1796$ μm, $d=15.5$ μm, $\Delta n=0.0098$, and $L=\Lambda/1.9$, where Δn is the index modulation amplitude superimposed to n_G and L the length of the polymerized unit cell. The only important dif-

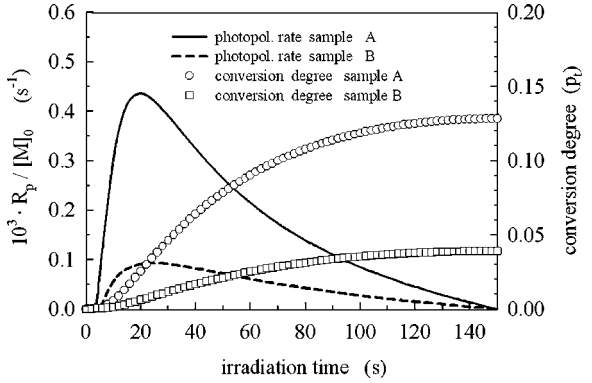

FIG. 6. Photopolymerization rates and conversion degrees as a function of the visible irradiation time for samples A (solid line and circle) and B (dashed line and square).

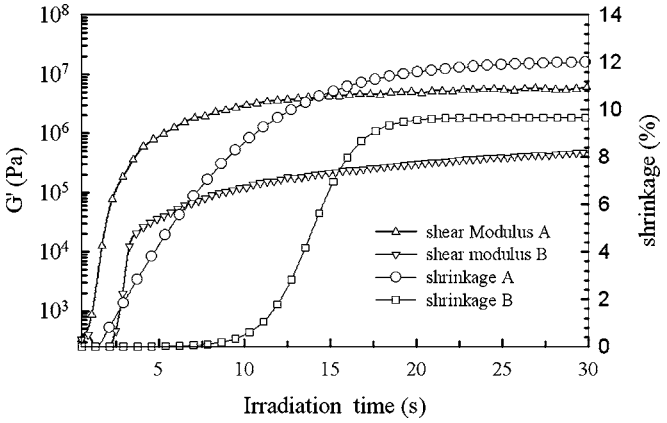

FIG. 7. The shear conservative modulus (G') and shrinkage as a function of the visible irradiation time for samples A (triangle up and circle) and B (triangle down and square).

ference with the experimental data concerns the two wide side lobes which can be easily attributed to the presence of inactivated photoinitiator species [19]. Therefore after subtraction from the experimental curve of the dye mixture contribution, the agreement between theory and experiment can be considered excellent.

The addition of the rhodamine dye in the mixture is responsible for a redshift of the position of the reflection peak as shown in Fig. 4. Changes in the refractive index of the mixture and in the grating pitch are both responsible for this peak shift and affect the observed shrinkage. More in detail, changes in the reflection peak position can be reasonably attributed to a reduced shrinkage effect ($\sim 3\%$ at 3×10^{-2} M) due to the presence of a high concentration of inert dye molecules. To prove our assertion a complete study of the photopolymerization kinetics of two mixtures, one without rhodamine (mixture A) and one with a 3×10^{-2} M concentration of rhodamine (mixture B), has been done as explained later. The transmission spectrum of a grating written using the mixture B is shown in Fig. 5 as dashed line. The presence of the rhodamine 6G dye is responsible for the strong absorption phenomenon observed in the left region of the spectrum. The continuous line represents the theoretical simulation of the reflection properties of the HPDLC grating made with the following parameters: $\Lambda = 0.1800$ μm, $d = 15.5$ μm, $\Delta n = 0.0055$, and $L = \Lambda/2$. As we can see, a reduction of the modulation amplitude and a modification of the length of the unit cells were necessary to best fit the experimental data points. These changes are consistent with a less efficient photopolymerization process which originates a periodic structure characterized by a lower dielectric contrast. Accordingly, the photopolymerization conversion degrees (p_t) and rates (R_p) as function of the irradiation time have been investigated for the VLC samples A and B (see Fig. 6). Since the photopolymerization rates and conversion degrees for the sample A are higher than B, these results confirm that the rhodamine 6G plays a photopolymerization inhibition effect probably due to a minor incident UV light reaching the photoinitiator system into the sample B under the same photopolymerization conditions. The well-known classical dependence between the photoinitiation rate (R_i) and the photopolymerization rate (R_p) is $R_p \propto (R_i)^{0.5} = (2\Phi I_a)^{0.5}$, where Φ and I_a are the efficiency and the amount of the absorbed light of the photoinitiator, respectively [14]. Although some authors have demonstrated that some deviations of this classical dependence are observed for some multi(meth)acrylate systems under diffusion controlled photopolymerization reactions, it is worth noting that R_i changes can strongly affect in any case the photopolymerization kinetic behavior [13,14].

Moreover, the optical shrinkage is due to the competition between the growth of the refractive index of the mixture during the photopolymerization and the shrinkage phenomenon. To distinguish between these two contributions we used the fast oscillating rotational rheometer to determine the effects on the shear mechanical moduli (G' or G'') induced by large internal stresses during the visible light curing of the samples after gelation [17]. The results of the photorheological measurements are reported in Fig. 7 for the visible light photocurable samples A and B. This figure suggests that the behavior of the shear mechanical moduli as a function of irradiation time is in agreement with that observed by using the photo-DSC technique. It is worth noting that the photopolymerization inhibition effect induces a minor shear mechanical conservative modulus (G') that leads to the shrinkage reduction observed in the sample B. The kinetic behavior influences even the gelation time, in fact the condition $\tan \delta = G''/G' = 1$ is achieved for samples A and B after 2.5 and 9.0 s, respectively. When the gelation time is reached, the initial liquid state of the photocurable sample has sufficiently transformed by photocrosslinking reactions into a stable highly viscous material maintaining its shape. Under these conditions the measured gap between the two plates gave a shrinkage of 12.0% and 9.5% for sample A and B, respectively. Even though the data are not directly comparable with those obtained from optical measurements, the general trend is clearly confirmed and in agreement with our starting assumptions of small changes in the refractive index of the mixtures after the photopolymerization processes. In principle these two techniques allow determining the real mechanical shrinkage of the mixture; further investigations are currently in progress to better quantify this statement.

V. CONCLUSIONS

Measurements of the linear mechanical shrinkage of several polymer-LC photopolymerizing mixtures have been done using two different experimental approaches. The general behavior of the experimental data under slight different polymerization conditions has provided consistent results confirming the starting hypothesis of small changes of the refractive index of the mixture after photopolymerization. Modifications in the reflection properties of the gratings as function of the active dye concentration have been determined experimentally and a detailed theoretical simulation of the transmission (and reflection) properties of these devices has been provided.

ACKNOWLEDGMENTS

This research was supported by EU Project No. E FP6-PLT-511568-3DTV. It has been performed within the frame of European STREP Project MICROHOLAS and of COST P8 Action.

[1] T. J. Bunning, L. V. Natarajan, V. P. Tondiglia, and R. Sutherland, Annu. Rev. Mater. Sci. **30**, 83 (2000).
[2] K. Tanaka, K. Kato, S. Tauru, and S. Sakai, J. Soc. Inf. Disp. **2/1**, 37 (1994).
[3] R. Jakubiak, T. J. Bunning, R. A. Vaia, L. V. Natarajan, and V. P. Tondiglia, Adv. Mater. (Weinheim, Ger.) **15**, 241 (2003).
[4] D. E. Lucchetta, L. Criante, O. Francescangeli, and F. Simoni, Appl. Phys. Lett. **84**, 4893 (2004).
[5] R. Jakubiak, L. V. Natarajan, V. P. Tondiglia, G. S. He, P. N. Prasad, T. J. Bunning, and R. Vaia, Appl. Phys. Lett. **85**, 6095 (2004).
[6] M. Notomi, H. Suzuki, and T. Tamamura, Appl. Phys. Lett. **78**, 1325 (2001).
[7] J. Qi, M. DeSarkar, G. T. Warren, and G. P. Crawford, J. Appl. Phys. **91**, 4795 (2002).
[8] R. L. Sutherland, L. V. Natarajan, V. P. Tondiglia, and T. J. Bunning, Chem. Mater. **5**, 1533 (1993).
[9] R. E. Collin, *Foundation for Microwave Engineering*, 2nd ed. (McGraw-Hill International Edition, New York, 1992).
[10] T. Rozzi and M. Mongiardo, *Open Electromagnetic Waveguides* (The Institution of Electrical Engineers, London, UK, 1997).
[11] C. Kittel, *Introduction to Solid State Physics*, 5th ed. (Wiley, New York, 1976).
[12] J. D. Jackson, *Classical Electrodynamics*, 2nd ed. (Wiley, New York, 1975).
[13] C. A. Guymon and C. N. Bowman, Macromolecules **30**, 1594 (1997).
[14] G. Odian, *Principles of Polymerization*, 3rd ed. (Wiley, London, 2004), Chap. 4.
[15] A. Turi, *Thermal Characterization of Polymeric Materials*, 2nd ed. (Academic Press, New York, 1997), Chap. 1.
[16] M. Bertoldo, S. Bronco, P. Narducci, S. Rossetti, and M. Scoponi, Macromol. Mater. Eng. **290**, 475 (2005).
[17] B.-S. Chiou, S. R. Raghavan, and S. A. Khan, Macromolecules **34**, 4526 (2001).
[18] J. Qi, E. Sousa, A. K. Fontecchio, and G. P. Crawford, Appl. Phys. Lett. **82**, 1652 (2003).
[19] D. E. Lucchetta, L. Criante, and F. Simoni, J. Appl. Phys. **93**, 9669 (2003).